LA-UR-16-27864 (Accepted Manuscript)

The arbitrary order mimetic finite difference method for a diffusion equation with a non-symmetric diffusion tensor

Gyrya, Vitaliy
Lipnikov, Konstantin

To be published in: Journal of Computational Physics

DOI to publisher's version: 10.1016/j.jcp.2017.07.019

Permalink to record: http://permalink.lanl.gov/object/view?what=info:lanl-repo/lareport/LA-UR-16-27864

Accepted Manuscript

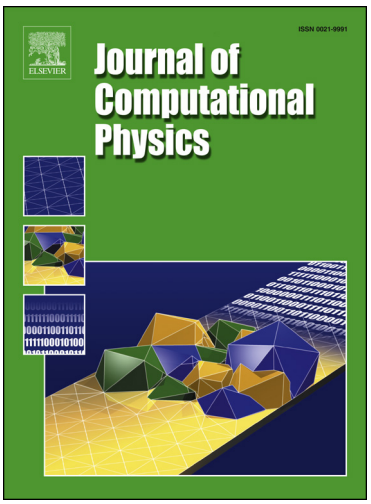

The arbitrary order mimetic finite difference method for a diffusion equation with a non-symmetric diffusion tensor

V. Gyrya, K. Lipnikov

PII: S0021-9991(17)30527-2
DOI: http://dx.doi.org/10.1016/j.jcp.2017.07.019
Reference: YJCPH 7466

To appear in: *Journal of Computational Physics*

Received date: 19 December 2016
Revised date: 2 June 2017
Accepted date: 10 July 2017

Please cite this article in press as: V. Gyrya, K. Lipnikov, The arbitrary order mimetic finite difference method for a diffusion equation with a non-symmetric diffusion tensor, *J. Comput. Phys.* (2017), http://dx.doi.org/10.1016/j.jcp.2017.07.019

The arbitrary order mimetic finite difference method for a diffusion equation with a non-symmetric diffusion tensor

V. Gyrya, K. Lipnikov

July 14, 2017

Abstract

We present the arbitrary order mimetic finite difference (MFD) discretization for the diffusion equation with non-symmetric tensorial diffusion coefficient in a mixed formulation on general polygonal meshes. The diffusion tensor is assumed to be positive definite. The asymmetry of the diffusion tensor requires changes to the standard MFD construction. We present new approach for the construction that guarantees positive definiteness of the non-symmetric mass matrix in the space of discrete velocities. The numerically observed convergence rate for the scalar quantity matches the predicted one in the case of the lowest order mimetic scheme. For higher orders schemes, we observed super-convergence by one order for the scalar variable which is consistent with the previously published result for a symmetric diffusion tensor. The new scheme was also tested on a time-dependent problem modeling the Hall effect in the resistive magnetohydrodynamics.

1 Introduction

The last decade has seen a development of a large number of discretization methods that work on unstructured polytopal (polygonal or polyhedral) meshes. Such meshes are in high demand in various engineering applications due to a critical flexibility they provide for working with complex geometries (e.g. subsurface flows). They appear as a result of mesh refinement, de-refinement, reconnection and other optimizations. They may also appear in multi-physics applications as dual to simpler meshes (e.g. Voronoi mesh as dual to a triangular mesh). In this time period, many discretization methods on polytopal meshes were extended to higher order. Higher-order schemes reduce significantly numerical diffusion which is critical for a number of multi-physics applications, e.g. for problems with dominated vorticity.

In this paper we present a new arbitrary order mimetic finite difference (MFD) method for diffusion problems with non-symmetric tensorial coefficients written in a mixed form.

This work revisits and extends the ideas developed in [14] for diffusion problems with symmetric tensors. The derivations are limited to polygonal meshes, although the underlying construction can be readily adjusted to polyhedral meshes.

The MFD method mimics important properties of the mathematical and physical systems such as conservation laws, symmetries, and duality of first-order differential operators. We refer readers to [14] for the discussion on the relationship between the MFD and other recently developed methods that can also work on polygonal meshes, such as the polygonal finite element (FE) methods [23, 20], hybrid high-order methods [5, 6], discontinuous Galerkin methods [7, 4], weak Galerkin method [17, 24], virtual element method [1, 3], mixed finite volume (FV) method [9, 8], hybrid FV method [11], discrete duality FV method [16], and gradient schemes [10]. We also refer interested readers to a review article [18] for a comprehensive historical overview of the development of mimetic schemes from classical finite differences to their present form.

Symmetry played a crucial role in the construction of the high-order mimetic schemes in our previous work [14], as well as in all prior mimetic schemes [18]. However, no extension to the case of a non-symmetric diffusion tensor has yet been done. This work addresses this shortcoming by analyzing various strategies for including asymmetry in a discrete scheme.

Although in most diffusion problems the diffusion tensor is symmetric (even isotropic), there exist a number of important applications that give rise to a non-symmetric diffusion tensor, e.g. in magnetohydrodynamics [21, 22, 25] and in ocean modeling for representing eddy-induced transport phenomena [12, 13]. In Section 5, we consider a mathematical model of plasma with the Hall effect which could be cast as the diffusion problem with a non-symmetric diffusion tensor. The asymmetry may also appear as the result of incorporating an advection term into a diffusion one, see Section 2.3. In our numerical experiments, we will consider elliptic and parabolic problems with a non-symmetric positive definite diffusion tensor that is either independent from solution or has the anti-symmetric component that is proportional to the solution.

The standard recipe for building mimetic schemes requires the mass matrix (in the space of discrete velocities) to satisfy two conditions: *(i)* the polynomial consistency and *(ii)* the spectral stability. Typically, one can write the cell-based mass matrix as a sum of two terms. The first term satisfies the consistency condition, but is a generate matrix for a general polytopal cell. The second term restores positive definiteness without breaking the consistency condition. Moreover, it guarantees uniform spectral bounds on shape regular meshes. This decomposition of the mass matrix can be viewed analogous to how a solution of an under-determined system can be written as a sum of a particular solution plus a general solution of the homogeneous system. The general solution is then selected in such a way to satisfy additional conditions, the spectral stability on our case.

In the case of a non-symmetric diffusion tensor, one can write two (left and right) consistency conditions, whereas in the symmetric case these conditions are identical. The right consistency condition is related to scheme accuracy, or its ability to satisfy the patch test, i.e. the scheme reproduces exactly polynomial solutions that belong to the approximation space. The left consistency condition becomes important when we want to solve efficiently

both the primary and dual diffusion problems. In this paper, we compare schemes with one and two consistence conditions. It appears that additional (the left) consistency condition can further improve (sometimes significantly) accuracy of the higher order schemes.

Efficient numerical solution of a diffusion problem is based on the hybridization of the mixed formulation. The hybridization procedure requires only inverse of the local mass matrix. Regardless of the number of employed consistency conditions, we can directly build the inverse of the mass matrix. The inverse matrix satisfies its own consistency conditions that are similar to that for the mass matrix; hence, it is built as the sum of the respected consistency and stability terms.

If for some reasons one needs a cell-based mass matrix, it can be easily build in a scheme based on only one (the right) consistency condition. For the schemes with two consistency conditions, we were unable to find a simple form for the stability term; hence, the construction of the inverse matrix has to be done first followed by its inversion.

The magnetohydrodynamics problem considered in Section 5 is the example of a problem with non-standard boundary conditions. In this problem, value of the normal derivative is specified on the boundary instead of a more conventional value of the flux which depends on the diffusion tensor. We extended the mimetic discretization technology to support such boundary conditions.

The rest of the paper is organized as follows. In Section 2 we present the elliptic and parabolic problems and write them in the mixed form. In Section 3 we present basic steps in the construction of mimetic schemes leaving details of the inner product matrix construction to Section 4. In Section 5 we present several numerical results that verify important properties of the mimetic schemes such as convergence rates and robustness on polygonal meshes. In Section 6 we make several concluding remarks. In the Appendix we present additional details that could help a reader with better understanding of some construction steps.

2 Problem statement

First, we consider a general elliptic problem and develop its mimetic discretization, since it contains major discretization challenges. Then, we extend the construction to parabolic problems by discretizing the accumulation term.

2.1 Elliptic problem

Consider a steady state diffusion problem in $\Omega \subset \mathbb{R}^d$ for a scalar variable p, referred to as the potential, with a scalar forcing term f and a diffusion tensor $\mathbb{K}$:

$$-\operatorname{div}(\mathbb{K}\nabla p) = f \quad \text{in} \quad \Omega,$$

subject to the boundary conditions on $\partial\Omega = \Gamma_D \cup \Gamma_N$:

$$\left\{ \begin{array}{rcll} p & = & g_D & \text{on} \quad \Gamma_D, \\ \mathbf{n} \cdot (\mathbb{K}\nabla p) & = & g_N & \text{on} \quad \Gamma_N, \end{array} \right. \tag{1}$$

where $\mathbf{n}$ is a unit outward normal. We will also consider a variant of the Neumann boundary condition of the form

$$\mathbf{n} \cdot \nabla p = g_N \quad \text{on} \quad \Gamma_N. \tag{2}$$

The Neumann boundary condition in (1) is the most natural choice, while condition (2) appears less often in physical systems and requires a more detailed discussion.

The diffusion coefficient $\mathbb{K}$ may not be symmetric, yet it is assumed to be strongly elliptic, i.e. there exists positive constants α_* and α^* such that

$$\alpha_* \|\mathbf{x}\|^2 \leq \mathbf{x}^T \mathbb{K}\, \mathbf{x} \leq \alpha^* \|\mathbf{x}\|^2 \qquad \text{for any } \mathbf{x} \in \mathbb{R}^d.$$

For the rest of the paper we will assume that $d = 2$; yet, the construction can be readily adjusted to $d = 3$ like it is done in [14] for the case of a symmetric tensor.

We rewrite the original equation in a mixed form using an auxiliary variable $\mathbf{u} = -\mathbb{K}\nabla p$, referred to as the velocity or flux:

$$\left\{ \begin{array}{rcl} \mathbb{K}^{-1}\mathbf{u} & = & -\nabla p \\ \operatorname{div}(\mathbf{u}) & = & f \end{array} \right. \quad \text{in} \quad \Omega. \tag{3}$$

The boundary conditions (1) are naturally written as boundary conditions for p and $\mathbf{u}$:

$$p = g_D \quad \text{on} \quad \Gamma_D, \qquad \text{and} \qquad \mathbf{n} \cdot \mathbf{u} = g_N \quad \text{on} \quad \Gamma_N.$$

The non-standard Neumann boundary condition (2) takes the following form:

$$\mathbf{n} \cdot \mathbb{K}^{-1}\mathbf{u} = g_N \quad \text{on} \quad \Gamma_N.$$

2.2 Parabolic problem

Discretization for a parabolic problem is the natural extension of that of an elliptic problem. Let

$$p_t - \operatorname{div}(\mathbb{K}\nabla p) = f \quad \text{in} \quad \Omega,$$

subject to boundary conditions (1) and the initial condition

$$p(0, \mathbf{x}) = g_0(\mathbf{x}) \quad \text{in} \quad \Omega.$$

The mixed formulation of the parabolic problem is written as

$$\left\{ \begin{array}{rcl} \mathbb{K}^{-1}\mathbf{u} & = & -\nabla p \\ p_t + \operatorname{div}(\mathbf{u}) & = & f \end{array} \right. \quad \text{in} \quad \Omega.$$

The boundary conditions for this formulation have the same form as in the elliptic case.

2.2.1 Time discretization of the parabolic system

Let us define velocity $\mathbf{u}^{n+\theta}$ for an integer n and a parameter $\theta \in [0,1]$ as the linear interpolation of two adjacent (in time) velocities $\mathbf{u}^n$ and $\mathbf{u}^{n+1}$:

$$\mathbf{u}^{n+\theta} = \theta \mathbf{u}^{n+1} + (1-\theta)\mathbf{u}^n.$$

The time discretization takes the following form:

$$\left\{ \begin{array}{lcl} \mathbb{K}^{-1}\mathbf{u}^{n+\theta} & = & -\nabla p^{n+\theta}, \\ \dfrac{p^{n+1}-p^n}{\triangle t} + \operatorname{div}(\mathbf{u}^{n+\theta}) & = & f^{n+\theta}. \end{array} \right. \tag{4}$$

The value of $\theta = 1$ corresponds to the implicit Euler discretization; $\theta = \frac{1}{2}$ corresponds to the Crank-Nicolson discretization; $\theta = 0$ corresponds to the explicit discretization.

2.3 Antisymmetric diffusion as advection

In this section we establish a link between the antisymmetric part of the diffusion tensor and the advection operator. Let $\mathbb{K}_a$ denote the antisymmetric part of $\mathbb{K}$:

$$\mathbb{K}_a := \frac{1}{2}\left(\mathbb{K} - \mathbb{K}^T\right) = \begin{bmatrix} 0 & \kappa_a \\ -\kappa_a & 0 \end{bmatrix},$$

where κ_a may be spatially dependent. Consider the term

$$\operatorname{div}(\mathbb{K}_a \nabla p) = \kappa_{a,x} p_y - \kappa_{a,y} p_x = \mathbf{curl}(\kappa_a) \cdot \nabla p.$$

When κ_a is curl-free, the antisymmetric part of the diffusion tensor has no contribution to the elliptic operator. In particular this is true for constant κ_a. For κ_a that is not curl-free the antisymmetric part $\mathbb{K}_a$ leads to a term that can be interpreted as the advection operator. In this case $\mathbf{curl}(\kappa_a)$ can be interpreted as a velocity.

Remark 1. *A converse of the above is also true. Any advection term that can be written in the form* $\mathbf{curl}(\kappa_a) \cdot \nabla p$ *can be rewritten as an antisymmetric part of the diffusion term and discretized using the approach of this paper.*

3 Mimetic finite difference method

Let us consider a sequence of shape-regular mesh partitions Ω_h characterized by the mesh size parameter h. On a mesh Ω_h, we define discrete analogs p_h, q_h and f_h of scalar functions p, q and f, and discrete analogs $\mathbf{u}_h$, $\mathbf{v}_h$ of vector functions $\mathbf{u}$, $\mathbf{v}$. They will be introduced formally in Section 3.2. We assume that p_h and q_h belong to the linear approximation space Q_h which is referred to as the space of scalar grid functions, and that $\mathbf{u}_h$ and $\mathbf{v}_h$ belong to the linear approximation space X_h, which is referred to as the space of flux grid functions.

We equip Q_h with the mimetic inner product $[\cdot,\cdot]_{Q_h}$, see Section 3.4 for more details, and X_h with the bilinear form $[\cdot,\cdot]_{X_h}$, see Section 3.6. Due to asymmetry of $\mathbb{K}$, the bilinear form $[\cdot,\cdot]_{X_h}$ is not an inner product. Instead, we will refer to it as the extended inner product, since all conditions other than symmetry are satisfied by it. The construction of the extended inner product is one of the main goals of this paper.

Let $\mathcal{DIV} : X_h \to Q_h$ be a discrete divergence operator which is introduced formally in Section 3.5. It approximates the continuous operator div. Furthermore, let $\widetilde{\mathcal{GRAD}} : Q_h \to X_h$ be a discrete gradient operator, see Section 3.8 for its construction. It approximates the combined operator $\mathbb{K}\nabla$. In the mimetic framework, the discrete divergence and gradient operators satisfy a discrete analogue of the Green formula.

Let $\widetilde{X}_h$ be a subspace of X_h of functions that satisfy the Neumann boundary conditions. The mixed MFD formulation for the elliptic system (3) reads: *Find* $p_h \in Q_h$ *and* $\mathbf{u}_h \in \widetilde{X}_h$ *such that*

$$\begin{cases} \mathbf{u}_h = -\widetilde{\mathcal{GRAD}}\, p_h, \\ \mathcal{DIV}\, \mathbf{u}_h = f_h. \end{cases}$$

3.1 Preliminary notations

We define $\mathcal{P}_l(E)$ as the space of polynomials on mesh polygon E of degree at most l. The dimension of the space $\mathcal{P}_l(E)$ is equal to $n_l^E = (l+1)(l+2)/2$. Here l is a generic integer and in the formulation of the method it may take different values. Let $\mathcal{M}^l(E) := \{m_{E,i}\}_{i=1,\dots,n_l^E}$ be a set of n_l^E scaled monomials forming a basis in $\mathcal{P}_l(E)$,

$$m_{E,i} = \left(\frac{x - x_{c,E}}{h_E}\right)^{\alpha_{i,x}} \left(\frac{y - y_{c,E}}{h_E}\right)^{\alpha_{i,y}}, \tag{5}$$

where $h_E = |E|^{\frac{1}{2}}$ scales like the diameter of cell E, $(x_{c,E}, y_{c,E})$ is its center of mass, and $(\alpha_{i,x}, \alpha_{i,y})$ is a multi-index such that $\alpha_{i,x}+\alpha_{i,y} \le l$. We assume ascending alphabetic ordering of the multi-index so that $m_{E,0} = 1$. The scaling in (5) simplifies enforcement of the spectral stability conditions. It leads to a simple scaling relation between matrices built on elements that can be obtained from one another by scaling, see Appendix B.

We define the projection operator $\Pi_l^E : L^2(E) \to \mathcal{P}_l(E)$ by the following conditions:

$$\int_E \Pi_l^E(u) p \; dE = \int_E u \; p \; dE \qquad \text{for all } p \in \mathcal{P}_l(E).$$

With a slight abuse of notation, we use the same symbol for the vector projection operator, $\Pi_l^E : (L^2(E))^d \to (\mathcal{P}_l(E))^d$, which is defined component-wise using the above formula.

For the mesh edge e and a non-negative integer number l, we take $P_l(e)$ to be the space of polynomials on e of degree up to l. The dimension of the space $P_l(e)$ is $n_l^e = l + 1$. Let $\mathcal{M}^l(e) := \{m_{e,i}\}_{i=1,\dots,n_l^e}$ be a set of scaled monomials forming a basis in $\mathcal{P}^l(e)$:

$$m_{e,i} = s^{i-1}, \tag{6}$$

where s defines the local variable for edge e. It is equal to zero at the edge center and ± 1 at the edge end points

We define the projection operator $\Pi_l^e : L^2(e) \to \mathcal{P}_l(e)$ by the following conditions:

$$\int_e \Pi_l^e(u) p \, dE = \int_e u \, p \, dE \qquad \text{for all } p \in \mathcal{P}_l(e).$$

When working with square matrices we will often find a need to extract their symmetric part. It will be convenient to introduce a shorthand notation for this

$$\mathbb{M}^S := \frac{1}{2}\left(\mathbb{M} + \mathbb{M}^T\right),$$

where $\mathbb{M}^T$ is the transpose of $\mathbb{M}$.

3.2 Degrees of freedom and local interpolation operators

Let $k > 0$ be an integer associated with the polynomial order of our scheme. For a cell E, the local approximation space Q_E consists of n_{k-1}^E DoF that are associated with the interior of the cell, see Fig. 1. The local interpolation operator $I : L^2(E) \to Q_E$ is defined using monomials (5) as follows

$$p_E^I = \left\{p_{E,i}^I\right\}_{i=1,\dots,n_{k-1}^E}, \quad p_{E,i}^I = \frac{1}{|E|}\int_E p \, m_{E,i} \, dE.$$

There is a one-to-one correspondence between Q_E and the space of polynomials $\mathcal{P}_{k-1}(E)$. The global approximation space Q_h is defined in terms of the local ones as

$$Q_h = \left\{p_h : \; p_h|_E \in Q_E\right\}, \tag{7}$$

where $p_h|_E$ is a restriction of p_h to cell E. Note that this definition does not include any boundary conditions.

For a cell E, the local approximation space X_E consists of two groups of DoFs (see Fig. 1):

- $(n_{k-1}^E - 1)$ degrees of freedom, $v_{E,i}^I$, associated with the interior of the cell;
- n_k^e degrees of freedom, $v_{e,i}^I$, associated with each edge e of the cell.

The local interpolation operator $I : L^2(E) \to X_E$ is defined separately for each group. For the internal DoFs, we use scaled monomials (5) except for $m_{E,0} = 1$:

$$v_{E,i}^I = \frac{h_E}{|E|}\int_E \mathbf{v} \cdot \nabla m_{E,i} \, dE. \tag{8}$$

For the edge DoF, we use monomials (6) and the fixed edge normal vector $\mathbf{n}_e$:

$$v_{e,i}^I = \frac{1}{|e|}\int_e (\mathbf{v} \cdot \mathbf{n}_e) \, m_{e,i} \, de. \tag{9}$$

The global approximation space X_h collects all unique DoF introduced above. The space $\widetilde{X}_h$ is the subspace of X_h that satisfies the Neumann boundary conditions discussed in Section 3.7.

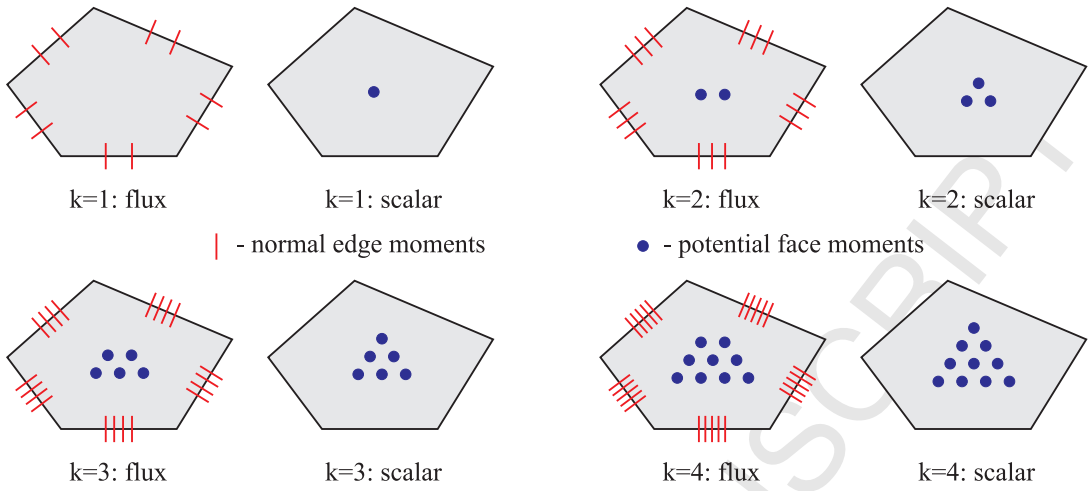

Figure 1: Degrees of freedom for approximation spaces Q_E and X_E for k=1,2,3,4.

3.3 Mesh regularity assumptions

A number of assumptions on the shape of mesh cells needs to be made for the numerical and theoretical analysis of the proposed schemes.

(MRA1) There exists a mesh independent number ρ_*, such that every cell E is star-shaped (i.e. visible from) with respect to every point of a circle of radius $\rho_* h_E$.

(MRA2) There exists a mesh independent number N_*, such that every cell E can be conformally partitioned into at most N_* shape-regular triangles T, i.e.

$$\rho_* h_T \leq r_T, \tag{10}$$

where r_T is the radius of the inscribed sphere in T and h_T is the diameter of T.

3.4 Inner product on Q_h

We start by defining the global inner product $[\cdot,\cdot]_{Q_h}$ as a sum of local contributions:

$$[p_h,\, q_h]_{Q_h} = \sum_E [p_h,\, q_h]_{Q_E}.$$

The local inner products $[\cdot,\cdot]_{Q_E}$ satisfy the consistency condition

$$[p_E^I,\, q_E^I]_{Q_E} = \int_E p\; q\; dE \quad \text{for all} \quad p, q \in \mathcal{P}_{k-1}(E). \tag{11}$$

Due to the one-to-one correspondence between Q_E and $\mathcal{P}_{k-1}(E)$, the local and, hence, the global inner products are well defined by (11). In the matrix form, the local inner product $[\cdot,\cdot]_{Q_E}$ is represented by a symmetric positive definite matrix $\mathbb{M}_{Q_E}$. The global inner product is represented by the block-diagonal matrix $\mathbb{M}_{Q_h}$ with as many blocks as there are mesh cells.

3.5 $\mathcal{DIV}$ operator

Hereafter, we consider mostly a single cell E. For each edge e of this E, we assume that $\mathbf{n}_e$ is the exterior normal. Orientation of the edge normals is important for the assembly of global operators and global matrices.

Let $\mathcal{DIV}_E$ denote the discrete divergence operator restricted to cell E. This operator is defined in such a way that it commutes with the interpolation operator, i.e. for any function $\mathbf{u}$ and its interpolant $\mathbf{u}_E^I \in X_E$, we have

$$\mathcal{DIV}_E \mathbf{u}_E^I = (\text{div } \mathbf{u})_E^I.$$

For any polynomial $p \in \mathcal{P}_{k-1}(E)$ and its interpolation $p_E^I \in Q_E$ we have

$$[\mathcal{DIV}_E \, \mathbf{u}_E^I, \, p_E^I]_{Q_E} = \int_E (\text{div } \mathbf{u}) \, p \, dE = - \int_E \mathbf{u} \cdot \nabla p \, dE + \sum_{e \in \partial E} \int_e (\mathbf{u} \cdot \mathbf{n}_e) p \, de. \tag{12}$$

Since p is a polynomial, the right-hand side of (12) can be written in terms of the DoF of $\mathbf{u}_E^I$. Thus, (12) defines the local (and hence the global) divergence operator uniquely.

3.6 Extended inner product on X_h

We define the global extended inner product $[\cdot, \cdot]_{X_h}$ as a sum of local extended inner products:

$$[\mathbf{v}_h, \, \mathbf{u}_h]_{X_h} = \sum_E [\mathbf{v}_h|_E, \, \mathbf{u}_h|_E]_{X_E}.$$

A key to the construction of an accurate local extended inner product lies in the consistency conditions. Due to asymmetry of the tensor $\mathbb{K}$, the extended inner products are no longer symmetric. As a consequence, instead of a single consistency condition, like in the previous mimetic schemes, we have two consistency conditions.

Consistency conditions: For all $p \in \mathcal{P}_{k+1}(E)$ and for all $\mathbf{v}$ such that $\text{div}\, \mathbf{v} \in \mathcal{P}_{k-1}(E)$ and $\mathbf{v} \cdot \mathbf{n} \in \mathcal{P}_k(e)$ for all edges $e \in \partial E$ we have

$$[(\Pi_k^E(\mathbb{K}^T \nabla p))^I, \, \mathbf{v}_E^I]_{X_E} = \int_E \nabla p \cdot \mathbf{v} \, dE, \tag{13}$$

$$[\mathbf{v}_E^I, \, (\Pi_k^E(\mathbb{K} \, \nabla p))^I]_{X_E} = \int_E \nabla p \cdot \mathbf{v} \, dE. \tag{14}$$

Hereafter (13) is referred to as the left and (14) as the right consistency conditions. Note that the space of functions $\mathbf{v}$ above is sufficiently rich so that $\mathbf{v}_E^I$ covers all of X_E. Also note that the right-hand side in both conditions is the same and can be computed without explicit knowledge of $\mathbf{v}$ inside cell E using only its DoF:

$$\int_E \nabla p \cdot \mathbf{v} \, dE = - \int_E p \, (\text{div}\, \mathbf{v}) \, dE + \sum_{e \in \partial E} \int_e p \, \mathbf{v} \cdot \mathbf{n} \, ds. \tag{15}$$

Thus, the right-hand side can be written as the dot products $\mathbf{r}_E(p)^T \mathbf{v}_E$ with computable vector $\mathbf{r}_E$ depending on polynomial p.

The right consistency condition is necessary and sufficient for scheme convergence. The left consistency condition is necessary when the primal and dual problems have to be solved simultaneously. Our numerical experiments indicate that it also improves significantly accuracy of the primal problem. We also observed a slightly higher convergence rate. The construction of the extended inner product is done in Section 4.

In addition to the consistency conditions, we require the stability conditions, which is formulated in terms of the matrix $\mathbb{M}_E$ corresponding to the local extended inner product $[\mathbf{u}_E^I, \mathbf{v}_E^I]_{X_E}$.

Stability conditions: There exists two positive constants α_0 and α_1 such that for any cell E and any vector $V \in X_E$ these two conditions are satisfied [19]:

$$\alpha_0 |E| \|V\|^2 \quad \leq V^T \mathbb{M}_E V, \tag{16}$$

$$\|\mathbb{M}_E V\| \leq \alpha_1 |E| \|V\|, \tag{17}$$

where $\|V\|$ indicates the Euclidean norm of V.

Remark 2. *Note that condition* (17) *implies*

$$|V^T \mathbb{M}_E V| \leq \alpha_1 |E| \|V\|^2 \tag{18}$$

but not the other way around, i.e. (17) *is stronger than* (18)*. The conditions* (16) *and* (18) *are both conditions on the symmetric part of the generalized inner product matrix* $\mathbb{M}_E$*, while* (17) *also bounds the asymmetric part of* $\mathbb{M}_E$*.*

3.7 Neumann boundary conditions

Typically, the Neumann boundary condition specifies the flux on the domain boundary. However, in some applications (e.g., see the resistive MHD problem in Section 5.2), the normal gradient of the solution may be specified. On the discrete level, in all cases the Neumann boundary conditions prescribe values to some DoF of $\mathbf{u}_h$, hence effecting the definition of the approximation space. For the conventional Neumann conditions, we prescribe the given flux values directly to the DoF:

$$\widetilde{X}_h = \Big\{ \mathbf{u}_h : \ \mathbf{u}_h|_E \in X_E \text{ and for } e \in \Gamma_N \ \ u_{e,\alpha} = \int_e g_N \, m_\alpha \, ds, \ \alpha = 0, \ldots, k \Big\}. \tag{19}$$

To approximate the non-standard Neumann boundary conditions, we need a local approximation of the gradient, i.e. $-\mathbb{K}^{-1}\mathbf{u}$. This approximation will be defined on each near-boundary cell as a linear map

$$\mathbb{L}_E : \mathbb{X}_E \to \mathbb{X}_E,$$

such that for any $\mathbf{u}_E, \mathbf{v}_E \in \mathbb{X}_E$ we have

$$[\mathbf{u}_E, \mathbf{v}_E]_{\mathbb{X}_E} = [[\mathbf{u}_E, \mathbb{L}_E \mathbf{v}_E]]_{\mathbb{X}_E}. \tag{20}$$

Here $[[\cdot,\,\cdot]]_{\mathbb{X}_E}$ is the inner product built the same way as the extended inner product $[\cdot,\,\cdot]_{\mathbb{X}_E}$, but the tensor $\mathbb{K}$ is replaced with the identity tensor. Thus, $[[\mathbf{u}_E^I,\,\mathbf{v}_E^I]]_{\mathbb{X}_E}$ approximates $\int_E \mathbf{u}\cdot\mathbf{v}\;dE$. Let $\widetilde{\mathbb{M}}_{X_E}$ be the matrix of the new inner product. Then, the linear map $\mathbb{L}_E$ is defined uniquely by (20) as

$$\mathbb{L}_E = \widetilde{\mathbb{M}}_{X_E}^{-1}\,\mathbb{M}_{X_E}.$$

For each $e\in\Gamma_N$ and the attached cell E, the non-standard Neumann boundary condition is written as

$$(\mathbb{L}_E\mathbf{u}_E)_{e,\alpha} = \int_e g_{\mathrm{N}}\,m_\alpha\;ds, \qquad \alpha = 0,\dots,k.$$

This equation can be used to eliminate the DoF corresponding to boundary edges from the final system. Formally, the global approximation space for the flux is defined as

$$\widetilde{X}_h = \Big\{\mathbf{u}_h\colon\ \mathbf{u}_h|_E\in X_E,\ \text{for } e\in\Gamma_N, e\in\partial E\ \ (\mathbb{L}_E\mathbf{u}_E)_{e,\alpha} = \int_e g_{\mathrm{N}}\,m_\alpha\;ds,\ \alpha=0,\dots,k\Big\}. \tag{21}$$

Remark 3. *Definition* (21) *reduces to definition* (19) *when we replace* $\mathbb{L}_E$ *with the identity matrix. This framework can be generalized to any boundary conditions of the form* $\mathbb{T}\nabla p\cdot\mathbf{n} = g_N$ *where* $\mathbb{T}$ *is a positive definite tensor.*

3.8 $\widetilde{\mathcal{GRAD}}$ operator and Dirichlet boundary conditions

We define operator $\widetilde{\mathcal{GRAD}}: Q_h\to X_h$ via a discrete version of the Green formula. This operator is the dual to operator $\mathcal{DIV}$ when the homogeneous Dirichlet boundary conditions are imposed on Γ_D. Recall that for a function $\mathbf{v}$ with zero normal component on Γ_N, we have

$$\int_\Omega \mathbf{v}\cdot\mathbb{K}^{-1}(\mathbb{K}\nabla p)\;d\Omega = -\int_\Omega (\operatorname{div}\mathbf{v})p\;d\Omega + \int_{\Gamma_D}(\mathbf{v}\cdot\mathbf{n})\,p\;ds.$$

Consider the interpolant $\mathbf{v}_h^I\in X_h$. Then for any $p_h\in Q_h$, we consider the following discrete Green formula:

$$[\mathbf{v}_h^I,\,\widetilde{\mathcal{GRAD}}\,p_h]_{X_h} = -[\mathcal{DIV}\,\mathbf{v}_h^I,\,p_h]_{Q_h} + \sum_{e\in\Gamma_D}\int_e (\mathbf{v}\cdot\mathbf{n})\,\Pi_k^e(g_D)\;ds. \tag{22}$$

The projection operator in the integrals over edges corresponding to the Dirichlet boundary conditions allows us to express them in terms of DoF of $\mathbf{v}_h^I$, see (9).

3.9 The forcing term f_h

The forcing term f_h is approximated on each cell E by taking its orthogonal projection onto polynomials of order $k-1$. For any piecewise polynomial function q such that $q|_E\in\mathcal{P}_{k-1}(E)$, we have the following identity

$$[f_h,\,q_h^I]_{Q_h} = \sum_E\int_E \Pi_{k-1}^E(f)\;q\;dE = \sum_E\int_E f\;q\;dE.$$

4 Extended inner product on space X_E

Recall that the extended inner product $[\cdot,\cdot]_{X_E}$ is represented by matrix $\mathbb{M}_{X_E}$. To simplify the notations, we shorten or drop completely the subscript, i.e. we write either $\mathbb{M}_E$ or $\mathbb{M}$.

Let us first rewrite the left-hand sides of (13) and (14) as vector-matrix-vector products and the right-hands sides as dot products of two vectors using (15). Since $\mathbf{v}_E$ is the arbitrary vector, we can cancel it to obtain the following matrix equations:

$$\mathbb{N}_l^T\,\mathbb{M} \;=\; \mathbb{R}^T, \tag{23}$$
$$\mathbb{M}\,\mathbb{N}_r \;=\; \mathbb{R}. \tag{24}$$

The columns of rectangular matrices $\mathbb{N}_l$ and $\mathbb{N}_r$ consist of DoF of L^2-projections $\Pi_k^E(\mathbb{K}^T\nabla p_i)$ and $\Pi_k^E(\mathbb{K}\nabla p_i)$, respectively, where $p_i = h_E\, m_{E,i}$, $i>1$:

$$\mathbb{N}_l = \left[N_{l,1},\ldots,N_{l,n_{k+1}^E-1}\right] \qquad \text{and} \qquad \mathbb{N}_r = \left[N_{r,1},\ldots,N_{r,n_{k+1}^E-1}\right],$$

The scaling coefficient h_E makes matrices $\mathbb{N}_l$ and $\mathbb{N}_r$ scale-invariant, see the Appendix for more details. The columns of $\mathbb{R}$ are vectors $R_i = \mathbf{r}_E(p_{i+1})$:

$$\mathbb{R} = \left[R_1,\ldots,R_{n_{k+1}^E-1}\right]. \tag{25}$$

It is important for subsequent derivations that matrix $\mathbb{R}$ does not depend on the diffusion tensor $\mathbb{K}$.

Lemma 1. *The matrices in the left and right consistency conditions (23) and (24) satisfy*

$$\mathbb{N}_l^T\mathbb{R} = \mathbb{R}^T\mathbb{N}_r =: \overline{\mathbb{K}}. \tag{26}$$

Moreover, $\overline{\mathbb{K}}$ is the positive definite matrix.

Proof. Let $p,q\in\mathcal{P}_{k+1}(E)$. Using the matrix form of the consistency conditions and definitions (13)-(14), we have

$$\begin{aligned} N_{l,i}^T R_j &= \int_E \Pi_k^E(\mathbb{K}^T\nabla p_{i+1})\nabla q_{j+1}\,dE = \int_E (\mathbb{K}^T\nabla p_{i+1})\cdot\nabla q_{j+1}\,dE,\\ R_i^T N_{r,j} &= \int_E \nabla p_{i+1}\cdot\Pi_k^E(\mathbb{K}\nabla q_{j+1})\,dE = \int_E \nabla p_{i+1}\cdot(\mathbb{K}\,\nabla q_{j+1})\,dE, \end{aligned}$$

where we used properties of the $L^2(E)$-projector in the last steps. The last integrals in both formulas are identical. Recall that the tensor $\mathbb{K}$ is positive definite, the basis functions p_i are linearly independent and their span does not contain a constant function. Using the argument by contradiction, we can easily show that the matrix $\overline{\mathbb{K}}$ is positive definite. This concludes the proof. □

Next we present two approaches to the construction of the inner product matrix $\mathbb{M}$. In the first approach, see Section 4.1, the inner product matrix satisfies only the right consistency condition (24) and in general does not satisfy the left consistency condition (23). In the second approach, see Section 4.2, the inner product matrix satisfies both consistency conditions. In Appendix A, we show that in the intuitive extension of the construction procedure from a symmetric tensor $\mathbb{K}$ to a non-symmetric one, it is difficult to enforce positive definiteness of $\mathbb{M}$. Instead, we will show how to construct a positive definite matrix $\mathbb{W} := \mathbb{M}^{-1}$. Recall that positive definiteness of $\mathbb{W}$ implies that of $\mathbb{M}$.

4.1 Satisfying right consistency condition only

Following closely to the conventional construction procedure [14], we build the inner product matrix $\mathbb{M}$ as the sum of the consistency, $\mathbb{M}_{\text{cons}}$, and stability, $\mathbb{M}_{\text{stab}}$, terms:

$$\mathbb{M} = \mathbb{M}_{\text{cons}} + \mathbb{M}_{\text{stab}}, \qquad \mathbb{M}_{\text{cons}} = \mathbb{R}\, \overline{\mathbb{K}}^{-1} \mathbb{R}^T. \tag{27}$$

Using Lemma 1, it is straightforward to verify that the consistency term satisfies the right consistency condition:

$$\mathbb{M}_{\text{cons}} \mathbb{N}_r = \mathbb{R}\, \overline{\mathbb{K}}^{-1} \mathbb{R}^T \mathbb{N}_r = \mathbb{R}\, \overline{\mathbb{K}}^{-1} \overline{\mathbb{K}} = \mathbb{R}.$$

The same lemma helps us to verify that $\mathbb{M}_{\text{cons}}$ also satisfies the left consistency condition.

The consistent term is only semi-positive definite, even for a triangular cell E. Its null space consists of vectors orthogonal to columns of $\mathbb{R}$. The stability term $\mathbb{M}_{\text{stab}}$ fixes this problem without breaking the consistency condition. The later means that

$$\mathbb{M}_{\text{stab}} \mathbb{N}_r = 0. \tag{28}$$

This orthogonality condition can be satisfied by writing the stability term as

$$\mathbb{M}_{\text{stab}} = \mathbb{D}_r \mathbb{S}\, \mathbb{D}_r^T, \qquad \mathbb{D}_r = \mathbb{I} - \mathbb{N}_r (\mathbb{N}_r^T\, \mathbb{N}_r)^{-1} \mathbb{N}_r^T, \tag{29}$$

where $\mathbb{S}$ is a positive definite matrix and $\mathbb{D}_r$ is the orthogonal compliment to $\mathbb{N}_r$, i.e. $\mathbb{D}_r^T\, \mathbb{N}_r = 0$ and square matrix $[\mathbb{D}_r,\, \mathbb{N}_r]$ has full rank.

Let us show that the resulting matrix $\mathbb{M}$ is positive definite. Using expressions (27) and (29) and orthogonality condition (28), we obtain

$$V^T \mathbb{M}\, V = V^T \mathbb{M}_{\text{cons}} V + V^T \mathbb{M}_{\text{stab}} V = V^T \mathbb{R}\, \overline{\mathbb{K}}^{-1} \mathbb{R}^T V + V^T \mathbb{D}_r\, \mathbb{S}\, \mathbb{D}_r^T V.$$

Both terms are semi-positive definite due to properties of matrices $\overline{\mathbb{K}}$ and $\mathbb{S}$. The stability term is zero only when $\mathbb{D}_r^T V = 0$; hence, $V = \mathbb{N}_r\, V_1$. The consistency term is zero only when $\mathbb{R}^T\, V = 0$; hence, $\mathbb{R}^T\, \mathbb{N}_r\, V_1 = 0$. Lemma 1 implies that $V_1 = 0$ and positive definiteness of the inner product matrix follows.

4.2 Satisfying both consistency conditions

Although matrix $\mathbb{M}_{\text{cons}}$ constructed in the previous section satisfies both consistency conditions the resulting matrix $\mathbb{M}$ in (27) is guarantied to satisfy only the right consistency condition due to the form of the stability term $\mathbb{M}_{\text{stab}}$. In the Appendix A we demonstrate that using the general form of the stability term $\mathbb{M}_{\text{stab}}$ that preserves both consistency conditions, it is not clear how to guaranty positive definiteness of the resulting matrix $\mathbb{M}$. Hence, there is a need for an alternative approach presented in this section.

We will perform the construction on an element with unit area. To obtain the matrix on a general element E one can first rescale the element, build the mass matrix on the rescaled element and multiply it by $|E|$. This construction is similar to the FE construction on a reference element and immediately implies independence of the condition number from the size of the element.

Let us rewrite consistency conditions (23)-(24) as the conditions for the inverse of the inner product matrix $\mathbb{W} = \mathbb{M}^{-1}$:

$$\mathbb{R}^T \mathbb{W} = \mathbb{N}_l^T, \tag{30}$$

$$\mathbb{W} \mathbb{R} = \mathbb{N}_r. \tag{31}$$

As before, we build matrix $\mathbb{W}$ as the sum of the consistency and stability terms:

$$\mathbb{W} = \mathbb{W}_{\text{cons}} + \mathbb{W}_{\text{stab}}, \quad \mathbb{W}_{\text{cons}} = \mathbb{N}_r \, \overline{\mathbb{K}}^{-1} \, \mathbb{N}_l^T \quad \text{and} \quad \mathbb{W}_{\text{stab}} = \mathbb{R}_\perp \, \mathbb{Z} \, \mathbb{R}_\perp^T, \tag{32}$$

where $\mathbb{Z}$ is a positive definite matrix, and $\mathbb{R}_\perp$ is the orthonormal compliment to $\mathbb{R}$, i.e. $\mathbb{R}^T \mathbb{R}_\perp = 0$, square matrix $[\mathbb{R}, \mathbb{R}_\perp]$ has full rank, and $\mathbb{R}_\perp^T \mathbb{R}_\perp = \mathbb{I}$. Note that the consistency term may not be positive definite in general. However, it is positive definite on the range of matrix $\mathbb{R}$, since $\mathbb{R}^T \, \mathbb{W}_{\text{cons}} \, \mathbb{R} = \overline{\mathbb{K}}$.

Using Lemma 1, it is straightforward to verify that matrix $\mathbb{W}$ satisfies both consistency conditions (30) and (31). Indeed, by the construction, the columns on $\mathbb{R}$ form the null space of the stability term:

$$\begin{aligned} \mathbb{R}^T \mathbb{W} &= \mathbb{R}^T \, \mathbb{W}_{\text{cons}} = \mathbb{R}^T \, \mathbb{N}_r \, \overline{\mathbb{K}}^{-1} \, \mathbb{N}_l^T = \mathbb{N}_l^T, \\ \mathbb{W} \mathbb{R} &= \mathbb{W}_{\text{cons}} \, \mathbb{R} = \mathbb{N}_r \, \overline{\mathbb{K}}^{-1} \, \mathbb{N}_l^T \, \mathbb{R} = \mathbb{N}_r. \end{aligned}$$

Remark 4. *The advantage of* (32) *versus a similar construction done for matrix* $\mathbb{M}$ *in Appendix A lies in the form of the stability term. In the construction for* $\mathbb{M}$*, it is difficult to enforce positive semi-definiteness of stability term* (52) *because* $\mathbb{D}_l \neq \mathbb{D}_r$ *in general, whereas in* (32) *positive semi-definiteness of* $\mathbb{W}_{stab}$ *is easy to control.*

Next, we will focus on satisfying the spectral stability conditions (and, in particular, positive definiteness) through a proper choice of the parameter matrix $\mathbb{Z}$. Consider a generic vector V and its decomposition into two orthogonal components:

$$V = \mathbb{R} \, V_{\mathbb{R}} + \mathbb{R}_\perp \, V_{\mathbb{R}_\perp}.$$

Then, we have

$$\begin{aligned} V^T \mathbb{W} V = V_{\mathbb{R}}^T (\mathbb{R}^T \mathbb{W}_{\text{cons}} \mathbb{R})\, V_{\mathbb{R}} + V_{\mathbb{R}_\perp}^T (\mathbb{R}_\perp^T\, \mathbb{W}_{\text{stab}}\, \mathbb{R}_\perp)\, V_{\mathbb{R}_\perp} + \\ + V_{\mathbb{R}}^T (\mathbb{R}^T \mathbb{W}_{\text{cons}} \mathbb{R}_\perp)\, V_{\mathbb{R}_\perp} + V_{\mathbb{R}_\perp}^T (\mathbb{R}_\perp^T \mathbb{W}_{\text{cons}} \mathbb{R})\, V_{\mathbb{R}} + V_{\mathbb{R}_\perp}^T (\mathbb{R}_\perp^T \mathbb{W}_{\text{cons}} \mathbb{R}_\perp)\, V_{\mathbb{R}_\perp}. \end{aligned} \tag{33}$$

The first two terms in (33) are non-negative by construction:

$$V_{\mathbb{R}}^T (\mathbb{R}^T \mathbb{W}_{\text{cons}} \mathbb{R})\, V_{\mathbb{R}} = V_{\mathbb{R}}^T\, \overline{\mathbb{K}}\, V_{\mathbb{R}} \geq 0 \quad \text{and} \quad V_{\mathbb{R}_\perp}^T (\mathbb{R}_\perp \mathbb{W}_{\text{stab}} \mathbb{R}_\perp)\, V_{\mathbb{R}_\perp} = V_{\mathbb{R}_\perp}^T \mathbb{Z}\, V_{\mathbb{R}_\perp} \geq 0. \tag{34}$$

The last three terms could be developed as follows

$$\begin{aligned} V_{\mathbb{R}}^T (\mathbb{R}^T \mathbb{W}_{\text{cons}}\, \mathbb{R}_\perp)\, V_{\mathbb{R}_\perp} &= V_{\mathbb{R}}^T (\mathbb{N}_l^T \mathbb{R}_\perp)\, V_{\mathbb{R}_\perp}, \\ V_{\mathbb{R}_\perp}^T (\mathbb{R}_\perp^T \mathbb{W}_{\text{cons}}\, \mathbb{R})\, V_{\mathbb{R}} &= V_{\mathbb{R}_\perp}^T (\mathbb{R}_\perp^T \mathbb{N}_r)\, V_{\mathbb{R}}, \\ V_{\mathbb{R}_\perp}^T (\mathbb{R}_\perp^T \mathbb{W}_{\text{cons}} \mathbb{R}_\perp)\, V_{\mathbb{R}_\perp} &= V_{\mathbb{R}_\perp}^T (\mathbb{R}_\perp^T \mathbb{N}_r)\, \overline{\mathbb{K}}^{-1} (\mathbb{N}_l^T \mathbb{R}_\perp)\, V_{\mathbb{R}_\perp}. \end{aligned} \tag{35}$$

Note that only the term (34) depends on the choice of the parameter matrix $\mathbb{Z}$, while three terms in (35) do not depend on the choice of $\mathbb{Z}$. Yet, the later three terms could be negative. In order to make the whole expression (33) positive, we should offset possible negative values using a stronger (in the spectral sense) matrix $\mathbb{Z}$.

We can rewrite (33) using (34) and (35) as

$$V^T\, \mathbb{W}\, V = \begin{bmatrix} V_{\mathbb{R}} \\ V_{\mathbb{R}_\perp} \end{bmatrix}^T \begin{bmatrix} \overline{\mathbb{K}} & \mathbb{N}_l^T \mathbb{R}_\perp \\ \mathbb{R}_\perp^T \mathbb{N}_r & \widetilde{\mathbb{Z}} \end{bmatrix} \begin{bmatrix} V_{\mathbb{R}} \\ V_{\mathbb{R}_\perp} \end{bmatrix}, \tag{36}$$

where

$$\widetilde{\mathbb{Z}} = \mathbb{Z} + (\mathbb{R}_\perp^T \mathbb{N}_r)\, \overline{\mathbb{K}}^{-1}\, (\mathbb{N}_l^T \mathbb{R}_\perp). \tag{37}$$

Thus, positivity of (33) is equivalent to showing that the square matrix in the right-hand side of (36) is positive definite. Positive definiteness of potentially non-symmetric matrix (36) is equivalent to positive definiteness of its symmetric part (we will choose $\mathbb{Z}$ in such a way that $\widetilde{\mathbb{Z}}$ is symmetric):

$$\begin{bmatrix} \overline{\mathbb{K}}_s & \mathbb{B} \\ \mathbb{B}^T & \widetilde{\mathbb{Z}} \end{bmatrix}, \qquad \begin{aligned} &\overline{\mathbb{K}}_s = \tfrac{1}{2}(\overline{\mathbb{K}} + \overline{\mathbb{K}}^T), \\ &\mathbb{B} = \mathbb{N}_s^T\, \mathbb{R}_\perp, \qquad \mathbb{N}_s := \tfrac{1}{2}(\mathbb{N}_l + \mathbb{N}_r). \end{aligned} \tag{38}$$

Recall the following linear algebra result for the Schur complement, see e.g. [2]. The symmetric matrix (38) is positive definite if and only if the first block $\overline{\mathbb{K}}_s$ and its Schur complement

$$\mathbb{H} := \widetilde{\mathbb{Z}} - \mathbb{B}^T\, \overline{\mathbb{K}}_s^{-1}\, \mathbb{B} \tag{39}$$

are both positive definite matrices. The matrix $\overline{\mathbb{K}}_s$ is positive definite by Lemma 1. The Schur complement $\mathbb{H}$ can be made positive definite by choosing $\widetilde{\mathbb{Z}}$ and, hence, $\mathbb{Z}$ appropriately.

In fact we can choose $\mathbb{H}$, which will imply the choice of the parameter matrix $\mathbb{Z}$ through formulas (39) and (37):

$$\begin{aligned}\mathbb{Z} &= \mathbb{H} + \mathbb{B}^T \overline{\mathbb{K}}_s^{-1} \mathbb{B} - (\mathbb{R}_\perp^T \mathbb{N}_r)\, \overline{\mathbb{K}}^{-1} (\mathbb{N}_l^T \mathbb{R}_\perp) = \\ &= \mathbb{H} + (\mathbb{R}_\perp^T \mathbb{N}_s)\, \overline{\mathbb{K}}_s^{-1} (\mathbb{N}_s^T \mathbb{R}_\perp) - (\mathbb{R}_\perp^T \mathbb{N}_r)\, \overline{\mathbb{K}}^{-1} (\mathbb{N}_l^T \mathbb{R}_\perp).\end{aligned} \tag{40}$$

The simplest choice for $\mathbb{H}$ is a scalar matrix, $\mathbb{H} = a\,\mathbb{I}$, with the appropriate value for parameter a. On one hand, a should be large enough so that $\mathbb{Z}$ is positive definite. On the other hand, the spectrum of $\mathbb{W}$ should be comparable to the spectrum of $\mathbb{W}_{\text{cons}}$. Taking

$$a = (1+\beta)\big\|\mathbb{W}_{\text{cons}}^S\big\|, \qquad \text{where } \beta > 0 \tag{41}$$

guaranties positive definiteness of $\mathbb{W}$. In Lemma 2 we will show uniform lower and upper bounds for this matrix which in turn lead to stability conditions (see Theorem 1). In fact, in our experiments taking $\beta = 0$ in (41) proved to be sufficient which could be also seen from Fig. 2.

Note that from (32), the expression (40) for $\mathbb{Z}$ with $\mathbb{H} = a\mathbb{I}$, and the orthonormality of columns of $\mathbb{Z}_\perp$, we can rewrite $\mathbb{W}_{\text{stab}}$ as follows

$$\mathbb{W}_{\text{stab}} = \mathbb{R}_\perp\, \mathbb{Z}\, \mathbb{R}_\perp^T = (\mathbb{R}_\perp \mathbb{R}_\perp^T) \left(a\mathbb{I} + (\mathbb{N}_s\, \overline{\mathbb{K}}_s^{-1} \mathbb{N}_s^T) - (\mathbb{N}_r\, \overline{\mathbb{K}}^{-1} \mathbb{N}_l^T) \right) (\mathbb{R}_\perp \mathbb{R}_\perp^T). \tag{42}$$

Note that $(\mathbb{R}_\perp \mathbb{R}_\perp^T)$ here is a projection operator that can be defined entirely in terms of $\mathbb{R}$ as

$$(\mathbb{R}_\perp \mathbb{R}_\perp^T) = \mathbb{I} - \mathbb{R}(\mathbb{R}^T\mathbb{R})^{-1}\mathbb{R}^T. \tag{43}$$

Lemma 2. *There exist two constants $\beta_1 > \beta_0 > 0$ such that for any element with unit area*

$$U^T\, \mathbb{W}\, U \;\; \geq \beta_0 \|U\|^2, \tag{44}$$

$$\beta_1 \|U\| \;\; \geq \|\mathbb{W}\, U\|. \tag{45}$$

We present a non-constructive proof that simply demonstrates existence of such constants $\beta_1 > \beta_0 > 0$ without giving an estimate of their values. Some estimate of these values could be obtained from Fig. 2 and the result of Theorem 1.

Proof. Consider the set $\mathcal{E}_n$ of elements E centered at the origin, with n vertices ordered counter clockwise and unit area. Any such element can be identified with a vector in $\mathbb{R}^{2n}$. Abusing notations we will consider $\mathcal{E}_n$ to be a subset of $\mathbb{R}^{2n}$. Define the distance between any two elements as the distance between the corresponding vectors in $\mathbb{R}^{2n}$.

The mesh regularity assumptions (MRA1) and (MRA2) of section 3.3 imply that all corresponding vectors belong to a finite ball. Moreover, the set $\mathcal{E}_n$ is closed, i.e. any limit point of $\mathcal{E}_n$ is in $\mathcal{E}_n$. Indeed, within any sequence E_i convergent to E there is a sub-sequence that in order to satisfy the mesh regularity assumptions uses *(i)* disks with convergent centers to satisfy star-shape regularity assumption (MRA1) and *(ii)* topologically the same

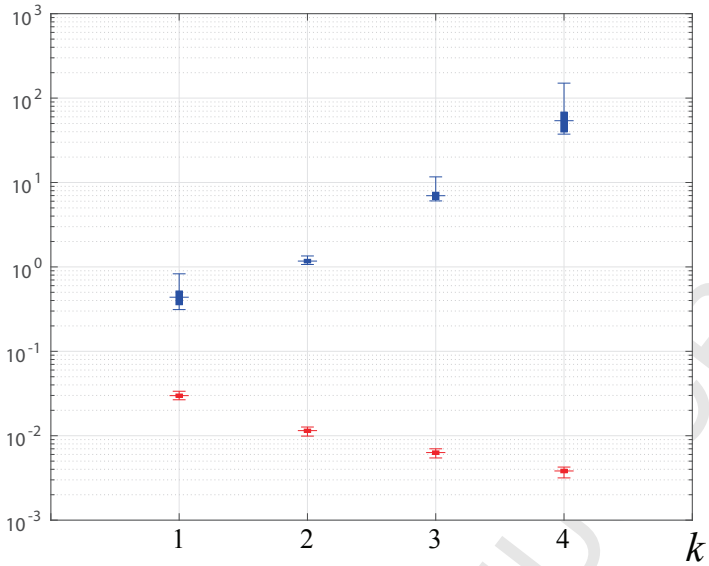

Figure 2: Estimates of the stability constants α_0 and α_1 in (16) and (17) on various perturbed quadrilaterals in the example of Section 5.1. The constant α_0 is estimated by taking the smallest eigenvalues (shown in red) of the symmetric part of the scaled matrix $|E|^{-1}\,\mathbb{M}_E$ for all cells E. The constant α_1 is estimated by taking the norm of the scaled matrix $|E|^{-1}\,\mathbb{M}_E$ for all cells E. For each $k = 1, \ldots, 4$, the plots show the two extreme observed values, the median and the standard deviation over 400 mesh cells.

triangular partition to satisfy (MRA2). Since both mesh regularity assumptions use non-strict inequalities, the limiting cell E naturally satisfies these assumptions with the limiting disk and partitions from *(i)* and *(ii)* above.

Since $\mathcal{E}_n$ is closed and bounded subset of $\mathbb{R}^{2n}$, it is compact, i.e. any infinite sequence contains a convergent sub-sequence.

Consider two functions as functions of E:

$$\beta_0(E) := \min_{\|U\|=1} \left\{ U^T\, \mathbb{W}_E\, U \right\}, \tag{46}$$

$$\beta_1(E) := \|\mathbb{W}_E\|. \tag{47}$$

Both functions are defined on $\mathcal{E}_n$ and are positive as was shown in the construction of $\mathbb{W}_E$ above. Also note that $\beta_0(E)$ and $\beta_1(E)$ are continuous functions of E. This can be verified by following the construction of $\mathbb{W}_E$ to see that all matrices involved in the construction depend continuously on the coordinates of the cell vertices. Indeed, these matrices are $\mathbb{R}$, $\mathbb{N}_l$, $\mathbb{N}_r$, $\overline{\mathbb{K}}$, and $\mathbb{H}$. The later one is a scalar matrix dependent on a defined in (41) and hence is continuous. Note that we were able to eliminate dependence of $\mathbb{W}_{\text{stab}}$ on $\mathbb{R}_\perp$ by using expressions (42) and (43).

Let us take β_0^n and β_1^n to be the lower and and upper bounds, respectively, for all cells in $\mathcal{E}_n$:

$$\beta_0^n := \inf_{E\in\mathcal{E}_n} \{\beta_0(E)\} \qquad \text{and} \qquad \beta_1^n := \sup_{E\in\mathcal{E}_n} \{\beta_0(E)\}. \tag{48}$$

From the compactness of $\mathcal{E}_n$, continuity of $\beta_0(\cdot)$ and $\beta_1(\cdot)$, and positivity of $\beta_0(E)$ for a general element E satisfying the mesh regularity assumptions, we conclude that $0 < \beta_0^n$ and $\beta_1^n < \infty$.

Let us take the minimum of β_0^n and the maximum of β_1^n over $n \leq N$, where N depends only on N_* introduced in assumption (MRA2):

$$\beta_1 := \max_{n=3,\dots,N} \{\beta_1^n\} \qquad \text{and} \qquad \beta_0 := \min_{n=3,\dots,N} \{\beta_0^n\}.$$

Since N is finite, we conclude that $\beta_1 < \infty$ and $\beta_0 > 0$. This completes the proof. □

Theorem 1. *Consider element with the unit area and set* $\mathbb{M} = \mathbb{W}^{-1}$. *This matrix satisfies the stability conditions (16)-(17) with*

$$\alpha_0 = \frac{\beta_0}{\beta_1^2} \qquad \textit{and} \qquad \alpha_1 = \frac{1}{\beta_0}.$$

Proof. Take $U = \mathbb{M}\, V$, hence, $V = \mathbb{W}\, U$ and rewrite conditions (16)-(17) in terms of $\mathbb{W}$ and U. The condition (17) states

$$\|U\| \leq \alpha_1 \|\mathbb{W}\, U\|.$$

The next inequality follows immediately from (44):

$$\beta_0 \|U\|^2 \leq U^T\, \mathbb{W}\, U \leq \|U\|\ \|\mathbb{W}\, U\|.$$

Hence, $\alpha_1 = 1/\beta_0$.

The condition (16) states

$$\alpha_0 \|\mathbb{W}\, U\|^2 \leq U^T\, \mathbb{W}\, U.$$

The next inequality follows from consecutive application of (45) and (44):

$$\|\mathbb{W}\, U\|^2 \leq \beta_1^2 \|U\|^2 \leq \frac{\beta_1^2}{\beta_0} U^T\, \mathbb{W}\, U.$$

Hence $\alpha_0 = \beta_0/\beta_1^2$. This proves the theorem. □

5 Numerical results

We consider two types of problems in this section. First, in Section 5.1, we consider the Poisson equation and estimate the convergence rates for various orders of approximation $k = 1, \dots, 4$. Then, in Section 5.2, we consider a nonlinear parabolic problem discretized with a second-order time integration scheme and the lowest order ($k = 1$) spatial discretization.

5.1 Poisson equation and convergence rates

Consider the stationary elliptic problem

$$\operatorname{div}(\mathbb{K}\nabla p) = f \quad \text{in} \quad \Omega = \left[-\tfrac{1}{2}, \tfrac{1}{2}\right] \times \left[-\tfrac{1}{2}, \tfrac{1}{2}\right]$$

subject to the Dirichlet boundary conditions $p = g$ on $\partial\Omega$. The non-symmetric diffusion tensor and the exact solution (see Fig. 3) are given by

$$\mathbb{K}(x,y) = \begin{bmatrix} K_{11} & K_{12} \\ K_{21} & K_{22} \end{bmatrix} = \begin{bmatrix} 1+x^2 & \sin(\pi x)y \\ -\sin(\pi x)y & 1+\frac{1}{2}y^2 \end{bmatrix}, \qquad p(x,y) = \sin(\pi x)y^2.$$

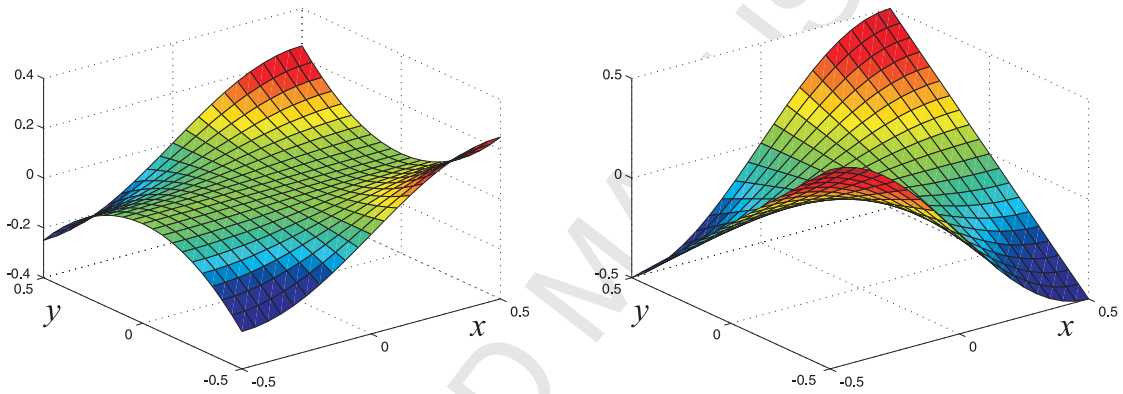

exact solution $p(x,y)$ $\qquad$ $K_{12}(x,y)$

Figure 3: Illustration of the exact solution and diffusion tensor component $K_{12}(x,y)$.

We ran simulations on perturbed square meshes, see Fig. 4. Each internal vertex is shifted along x- and y-axis by a uniform random variable taking values in the interval $[-\frac{h}{4}, \frac{h}{4}]$. To reduce impact of the random variable on the calculated error, we perform ten simulations for each value of $k = 1, 2, 3, 4$ and each value of the mesh resolution parameter h. The calculated error is averaged and plotted on Fig. 5 and 6. The error values and standard deviations as well as the averaged values are shown in Tables 1 and 2.

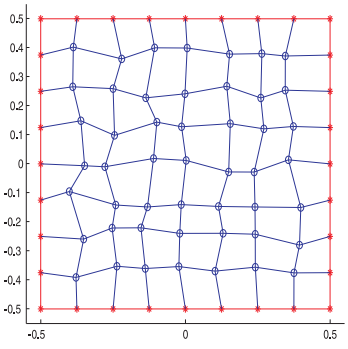

Figure 4: Sample mesh.

Note that the standard deviation values do not indicate uncertainty in our calculations, but rather variations in the error as a function of the mesh variability. As can be seen from Tables 1 and 2, the standard deviation values are typically less than 10% of the calculated error, although at times could be as large as $20\% - 25\%$, e.g. for $k = 4$ and $h = 2^{-2}, 2^{-3}$.

The convergence rate for the flux exhibits small variations and closely follows h^{k+1} formula. The convergence rate for the scalar variable, on the other hand, looks more interesting.

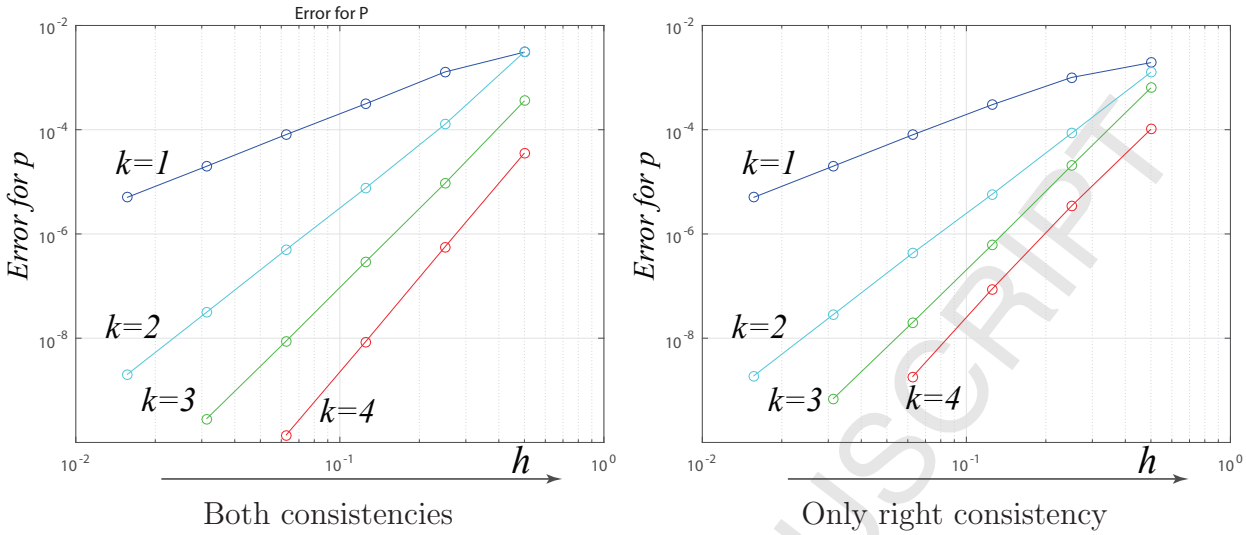

Figure 5: The L^2-error and convergence rates for the scalar variable p. Left panel: both consistency conditions are satisfied. Right panel: only the right consistency condition is satisfied.

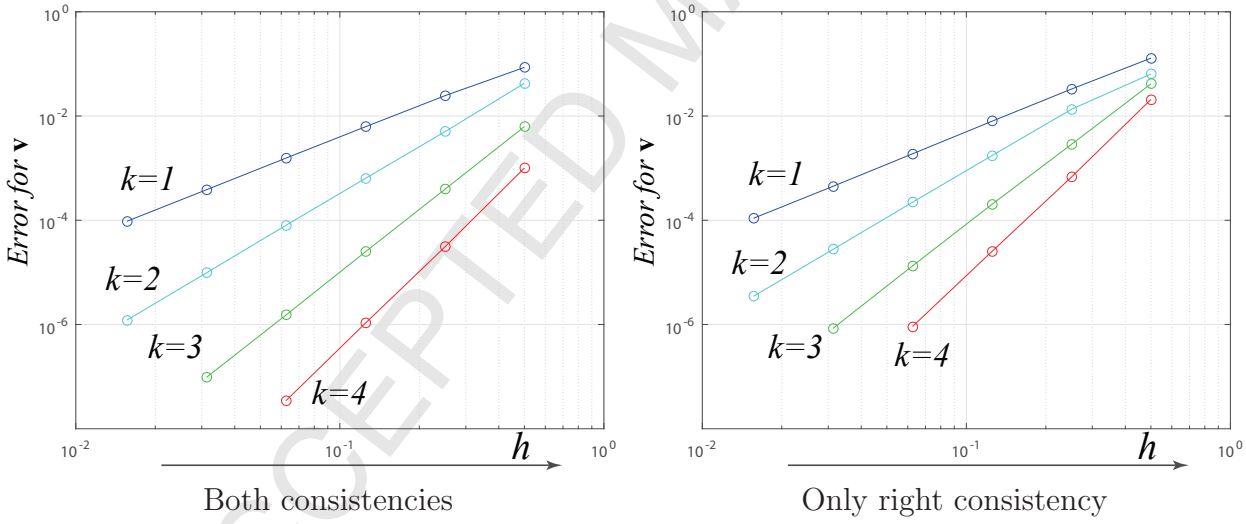

Figure 6: The discrete error and convergence rates for the flux variable $\mathbf{u}$. Left panel: both consistency conditions are satisfied. Right panel: only the right consistency condition is satisfied.

On one hand, it exhibits ultra-convergence for $k \geq 2$, with error of h^{k+2}. On the other hand, fluctuations in the error for scalar variable as a function of mesh are about 2-2.5 times larger than for the flux.

Finally, we observe that schemes with two consistency conditions lead to much more accurate solution, especially for the flux variable, for $k \geq 2$.

Table 1: The L^2 error, $\|p_h - p^I_{\text{exact}}\|_{Q_h}$, for the scalar variable p_h and the convergence rates estimated based on the first and last simulation for a particular value of $k = 1, 2, 3, 4$.

	$\mathbf{h = 2^{-1}}$	$\mathbf{h = 2^{-2}}$	$\mathbf{h = 2^{-3}}$	$\mathbf{h = 2^{-4}}$	$\mathbf{h = 2^{-5}}$	$\mathbf{h = 2^{-6}}$	**rate**
k = 1	3.08×10^{-3}	1.28×10^{-3}	3.13×10^{-4}	8.04×10^{-5}	1.98×10^{-5}	5.02×10^{-6}	**1.85**
	$\pm 6.65 \times 10^{-4}$	$\pm 2.72 \times 10^{-4}$	$\pm 3.95 \times 10^{-5}$	$\pm 1.38 \times 10^{-6}$	$\pm 1.55 \times 10^{-7}$	$\pm 2.15 \times 10^{-8}$	
k = 2	3.12×10^{-3}	1.27×10^{-4}	7.53×10^{-6}	4.97×10^{-7}	3.13×10^{-8}	2.00×10^{-9}	**4.11**
	$\pm 1.46 \times 10^{-4}$	$\pm 1.69 \times 10^{-5}$	$\pm 7.68 \times 10^{-7}$	$\pm 3.81 \times 10^{-8}$	$\pm 1.02 \times 10^{-9}$	$\pm 2.46 \times 10^{-11}$	
k = 3	3.57×10^{-4}	9.35×10^{-6}	2.90×10^{-7}	8.72×10^{-9}	2.83×10^{-10}	–	**5.07**
	$\pm 3.67 \times 10^{-5}$	$\pm 1.36 \times 10^{-6}$	$\pm 2.51 \times 10^{-8}$	$\pm 3.12 \times 10^{-10}$	$\pm 3.97 \times 10^{-12}$	–	
k = 4	3.56×10^{-5}	5.63×10^{-7}	8.49×10^{-9}	1.37×10^{-10}	–	–	**6**
	$\pm 3.39 \times 10^{-6}$	$\pm 4.75 \times 10^{-8}$	$\pm 5.19 \times 10^{-10}$	$\pm 6.82 \times 10^{-12}$	–	–	

Table 2: Error $\|\mathbf{v}_h - \mathbf{v}^I_{\text{exact}}\|_{X_h}$ for the flux variable and the convergence rates estimated based on the first and last simulation for a particular value of $k = 1, 2, 3, 4$.

	$\mathbf{h = 2^{-1}}$	$\mathbf{h = 2^{-2}}$	$\mathbf{h = 2^{-3}}$	$\mathbf{h = 2^{-4}}$	$\mathbf{h = 2^{-5}}$	$\mathbf{h = 2^{-6}}$	**rate**
k = 1	8.57×10^{-2}	2.45×10^{-2}	6.22×10^{-3}	1.56×10^{-3}	3.85×10^{-4}	9.58×10^{-5}	**1.96**
	$\pm 1.50 \times 10^{-3}$	$\pm 1.84 \times 10^{-3}$	$\pm 1.61 \times 10^{-4}$	$\pm 1.36 \times 10^{-5}$	$\pm 2.74 \times 10^{-6}$	$\pm 3.13 \times 10^{-7}$	
k = 2	4.25×10^{-2}	5.00×10^{-3}	6.36×10^{-4}	8.00×10^{-5}	9.79×10^{-6}	1.22×10^{-6}	**3.02**
	$\pm 1.24 \times 10^{-3}$	$\pm 4.15 \times 10^{-4}$	$\pm 2.95 \times 10^{-5}$	$\pm 1.39 \times 10^{-6}$	$\pm 6.38 \times 10^{-8}$	$\pm 3.04 \times 10^{-9}$	
k = 3	6.25×10^{-3}	3.93×10^{-4}	2.48×10^{-5}	1.52×10^{-6}	9.70×10^{-8}	–	**3.99**
	$\pm 4.79 \times 10^{-4}$	$\pm 2.69 \times 10^{-5}$	$\pm 1.20 \times 10^{-6}$	$\pm 3.39 \times 10^{-8}$	$\pm 1.35 \times 10^{-9}$	–	
k = 4	1.00×10^{-3}	3.08×10^{-5}	1.06×10^{-6}	3.45×10^{-8}	–	–	**4.94**
	$\pm 1.42 \times 10^{-4}$	$\pm 2.09 \times 10^{-6}$	$\pm 6.34 \times 10^{-8}$	$\pm 1.13 \times 10^{-9}$	–	–	

5.2 Hall effect

In this section we consider the resistive magnetohydrodynamics problem with the Hall effect presented in [15]. For completeness of the presentation, we repeat the problem formulation. Let B be the z-component of the magnetic field that satisfies the following equation:

$$B_t - \frac{1}{\mu_0}\,\text{div}\left(\frac{1}{\sigma}\nabla B\right) - \frac{1}{|q_e|\mu_0}\,\text{curl}\left(\frac{1}{n}B\nabla B\right) = 0 \qquad \text{in } \Omega,$$

subject to the initial and boundary conditions:

$$\begin{aligned} B(0) &= B_0 && \text{in } \Omega = [-.5, .5]^2, \\ B &= B_{\text{top}} && \text{on } \Gamma_{\text{top}}, \\ \mathbf{n}\cdot\nabla B &= 0 && \text{on } \Gamma_{\text{left}} \cup \Gamma_{\text{bottom}} \cup \Gamma_{\text{right}}, \end{aligned}$$

where Γ_{left}, Γ_{bottom}, Γ_{right} and Γ_{top} indicate the left, bottom, right and top sides of the square domain Ω. After the following non-dimensionalization,

$$\begin{aligned} &\lambda_{\text{r}} = c t_{\text{r}}, \\ &t_{\text{r}} = \omega_{\text{p}}^{-1} = \left(\frac{n_{\text{r}}|q_e|^2}{\varepsilon_0 m_{\text{e}}}\right)^{-1/2}, \qquad \text{where } \omega_{\text{p}} \text{ is the plasma frequency,} \\ &B_r = \frac{m_{\text{e}}}{|q_e| t_{\text{r}}}, \end{aligned}$$

and change of variables, $p := B/B_{\rm r}$, the original equation reduces to

$$p_t - \operatorname{div}(\mathbb{K}(p)\nabla p) = 0 \qquad \text{in} \quad (0,T)\times\Omega, \qquad \Omega = \left[-\tfrac{1}{2},\tfrac{1}{2}\right]\times\left[-\tfrac{1}{2},\tfrac{1}{2}\right], \tag{49}$$

with the solution-dependent diffusion tensor

$$\mathbb{K}(p) = \begin{bmatrix} \alpha & \beta p \\ -\beta p & \alpha \end{bmatrix}, \qquad \alpha = \frac{\varepsilon_0\omega_{\rm p}}{\sigma}, \qquad \beta = \frac{n_{\rm r}}{n}.$$

We chose to consider the time interval from 0 to $T = 0.5t_{\rm r}$. The initial condition is

$$p(t=0) = p_0 = \begin{cases} 0 & y < 0 \\ -1 & y > 0 \end{cases} \tag{50}$$

and the boundary conditions are

$$\begin{aligned} p &= -1 \quad \text{on } \Gamma_{\rm top}, \\ \nabla p\cdot\mathbf{n} &= 0 \quad \text{on } \Gamma_{\rm left}\cup\Gamma_{\rm right}\cup\Gamma_{\rm bottom}. \end{aligned}$$

The spatially dependent material parameters are taken to be

$$\alpha(x) = \begin{cases} 10^{-2} & \text{for } x<0, \\ 10^{-3} & \text{for } x>0, \end{cases} \qquad \beta(x) = \begin{cases} 10^{-1} & \text{for } x<0, \\ 10^{-5} & \text{for } x>0. \end{cases} \tag{51}$$

The material parameter α indicates stronger diffusion in the left half of the computational domain. The jump in the antisymmetry parameter β is ultimately responsible for the formation of the spike along the material interface in the solution, see Fig. 7. This spike would form even if the parameter α was constant throughout the whole domain and did not experience discontinuity at the interface $x = 0$. The formation of the spike is known as the Hall effect.

The time discretization was done using both the Crank-Nicolson ($\theta = \frac{1}{2}$) and the backward Euler ($\theta = 1$) schemes (see formula (4)) with no visible effect on the final discrete solution. In all cases, the value of the diffusion coefficient $\mathbb{K}(p)$ was computed using solution p at the last known time step. The spatial discretization step was taken to be $\triangle x = \triangle y = 2^{-6} = 1/64$. The temporal discretization step was taken to be $\triangle t = 0.01t_{\rm r}$.

In the left ($x < 0$) and right ($x > 0$) parts of the computational domain, we observe diffusion of the initial step-function profile (50), with the diffusion being faster in the left part (see values of $\alpha(x)$). At the material interface ($x = 0$) we observe the Hall effect, i.e. advance of the high gradient values along the interface. The numerical solution captures this effect and is visually identical to the reference solution obtained in [15].

We also performed the same numerical experiment on the unstructured Voronoi mesh adapted to the solution, see Fig. 8. The polygonal mesh contains 8196 vertices, 12292 edges and 4097 polygonal cells. More precisely, the mesh contains 1 triangle, 22 quadrilaterals, 379 pentagons, 3475 hexagons, 204 heptagons, and 16 octagons. Note that the number of mesh cells in this experiment is close to that in the previous experiment.

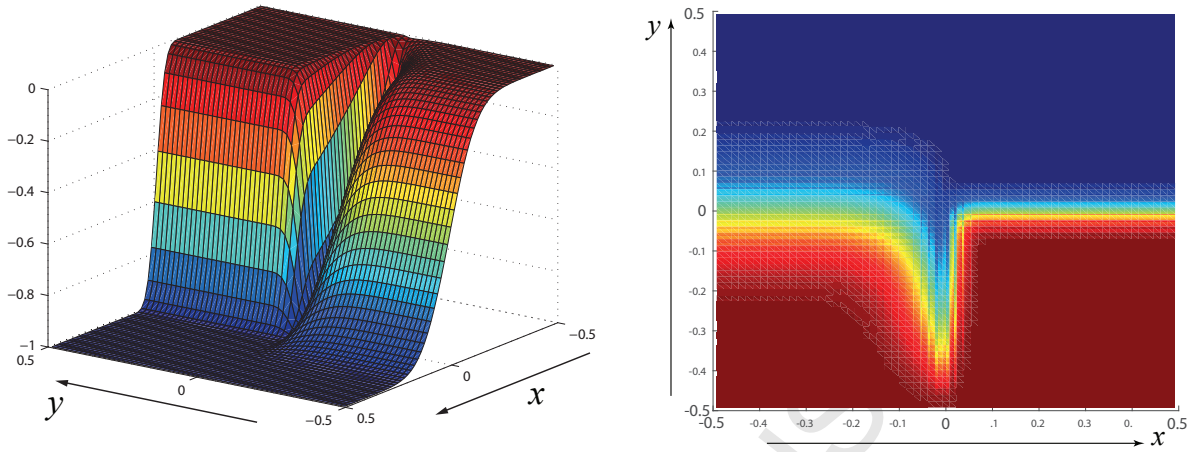

Figure 7: The side and top views of the numerical solution to problem (49)-(51) at time $T = 0.5t_{\rm r}$ on a 64×64 mesh.

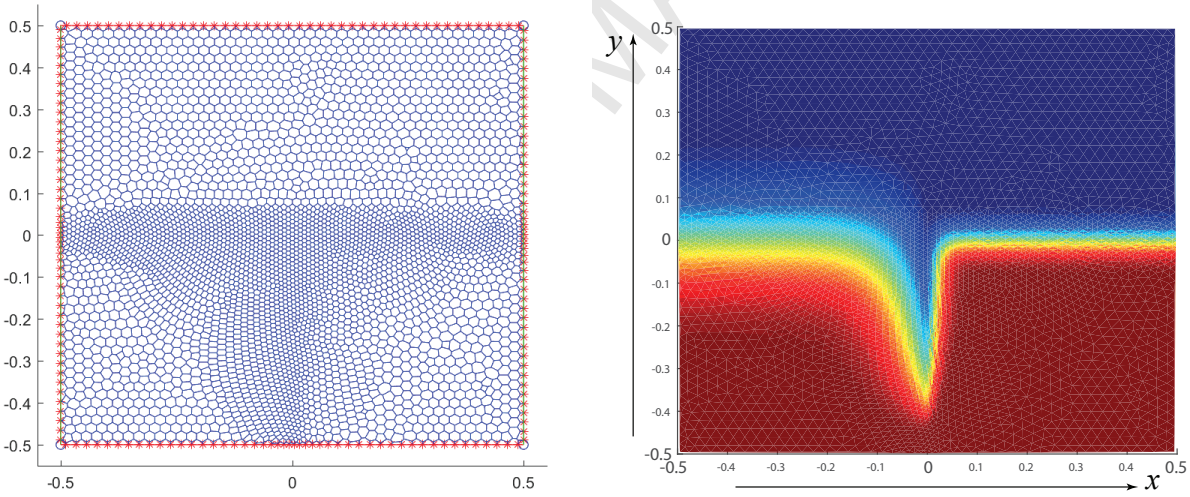

Figure 8: The adaptive unstructured Voronoi mesh (left panel) and the numerical solution (right panel).

6 Conclusions

We extended the mimetic finite difference method to elliptic problems with non-symmetric diffusion tensors. More specifically, we developed arbitrary order mimetic schemes that enforce one or two consistency conditions. For the case of two consistency conditions, we developed the new algorithm for building positive definite inner product matrices.

The numerical experiments demonstrated that enforcing only one consistency condition

was sufficient for convergence of the mimetic schemes. However, comparison with the schemes that enforce two consistency conditions had shown interesting phenomena. There was no difference in convergence rates for the lowest order discretizations. For higher order discretizations, the scheme with both consistency conditions resulted in a much smaller error. An extensive theoretical analysis is required to explain this behavior.

We tested the new schemes on both elliptic and parabolic problems. The parabolic problem was taken from the resistive magnetohydrodynamics with the Hall effect. We were able to capture this effect using the lowest-order spatial discretization ($k = 1$) and both the backward Euler and Crank-Nicolson time integration schemes.

Acknowledgements

This work was partially supported by the National Nuclear Security Administration of the U.S. Department of Energy at Los Alamos National Laboratory under Contract No. DE-AC52-06NA25396 and the DOE Office of Science Advanced Scientific Computing Research (ASCR) Program in Applied Mathematics.

A Conventional approach to constructing the inner product matrix

In this section, we discuss problems with the conventional approach (see Section 4.1) to the construction of the extended inner product matrix that satisfy the left and right consistency conditions. Let us try to build this matrix as the sum of the consistency and stability terms, like in formula (27). Ultimately, this approach does not work due to difficulties with enforcing positive definiteness of the matrix, which is the valuable insight in our opinion.

The consistency term $\mathbb{M}_{\text{cons}}$ is built the same way as in (27) and satisfies both consistency conditions (23) and (24). To ensure non-interference with both consistency conditions, the stability term must be both the right-orthogonal to $\mathbb{N}_r$ and the left-orthogonal to $\mathbb{N}_l$, i.e.

$$\mathbb{N}_l^T \mathbb{M}_{\text{stab}} = 0 \qquad \text{and} \qquad \mathbb{M}_{\text{stab}} \mathbb{N}_r = 0.$$

Hence, the general form of this term is (compare with (29))

$$\mathbb{M}_{\text{stab}} = \mathbb{D}_l \, \mathbb{S} \, \mathbb{D}_r^T, \tag{52}$$

where $\mathbb{D}_l$ and $\mathbb{D}_r$ are orthogonal compliments to $\mathbb{N}_l$ and $\mathbb{N}_r$, respectively, i.e. $\mathbb{D}_l^T \mathbb{N}_l = 0 = \mathbb{D}_r^T \mathbb{N}_r$ and square matrices $[\mathbb{D}_l, \mathbb{N}_l]$ and $[\mathbb{D}_r, \mathbb{N}_r]$ have full ranks. The square matrix $\mathbb{S}$ must be chosen wisely to guarantee positive definiteness of the inner product matrix $\mathbb{M}$. Take an arbitrary vector V and consider its decomposition of the form

$$V = \mathbb{R} \, V_{\mathbb{R}} + \mathbb{R}_\perp \, V_{\mathbb{R}_\perp}. \tag{53}$$

Using the expressions for $\mathbb{M}_{\text{cons}}$ and $\mathbb{M}_{\text{stab}}$, we have

$$V^T \mathbb{M} V = V_{\mathbb{R}}^T \overline{\mathbb{K}}^{-1} V_{\mathbb{R}} + V_{\mathbb{R}}^T (\mathbb{R}^T \mathbb{D}_l) \mathbb{S} (\mathbb{D}_r^T \mathbb{R}) V_{\mathbb{R}} + V_{\mathbb{R}}^T (\mathbb{R}^T \mathbb{D}_l) \mathbb{S} (\mathbb{D}_r^T \mathbb{R}_\perp) V_{\mathbb{R}_\perp} + V_{\mathbb{R}_\perp}^T (\mathbb{R}_\perp^T \mathbb{D}_l) \mathbb{S} (\mathbb{D}_r^T \mathbb{R}) V_{\mathbb{R}} + V_{\mathbb{R}_\perp}^T (\mathbb{R}_\perp^T \mathbb{D}_l) \mathbb{S} (\mathbb{D}_r^T \mathbb{R}_\perp) V_{\mathbb{R}_\perp}.$$

The first term is always non-negative. Unfortunately, it is not clear how to enforce positivity of the remaining terms.

Remark 5. *Although the consistency conditions (30)-(31) for $\mathbb{W} = \mathbb{M}^{-1}$ look similar to the consistency conditions (23)-(24) for $\mathbb{M}$, the difference in the structure of the stability terms is critical:*

$$\mathbb{M}_{stab} = \mathbb{D}_l \mathbb{S} \mathbb{D}_r^T, \quad \mathbb{W}_{stab} = \mathbb{R}_\perp \mathbb{Z} \mathbb{R}_\perp^T.$$

The stability term $\mathbb{W}_{stab}$ is semi-positive definite by design when $\mathbb{Z}$ is positive definite.

B Scaling considerations

Consider two polygonal cells E and E_1, where $|E| = h^2$, $|E_1| = 1$ and E_1 is obtained by isotropic scaling of E. Let p_1 and $\mathbf{v}_1$ be a scalar and a vector functions, respectively, defined on E_1. Define function p and $\mathbf{v}$ on E by

$$p(x,y) = p_1\left(\frac{x}{h}, \frac{y}{h}\right) \qquad \mathbf{v}(x,y) = \mathbf{v}_1\left(\frac{x}{h}, \frac{y}{h}\right). \tag{54}$$

That is, if one was to plot these functions, the plots for p and $\mathbf{v}$ would look like plots for p_1 and $\mathbf{v}_1$ scaled in x- and y-directions by a factor of h.

Let us study how the local interpolants of these functions as well as various integrals are related to one another. We start with the following observations:

$$\frac{1}{h^2} \int_E p(x) \left(\frac{x}{h}\right)^{\alpha_x} \left(\frac{y}{h}\right)^{\alpha_y} \, dxdy = \int_{E_1} p_1(x) x^{\alpha_x} y^{\alpha_y} \, dxdy \tag{55}$$

and

$$\int_{-1}^{1} p(x(s))\, s^{\alpha_s} \, ds = \int_{-1}^{1} p_1(x(s))\, s^{\alpha_s} \, ds. \tag{56}$$

We also have

$$\frac{1}{h} \int_E p(x) \nabla \left(\frac{x}{h}\right)^{\alpha_x} \left(\frac{y}{h}\right)^{\alpha_y} \, dxdy = \int_{E_1} p_1(x) \nabla \left(x^{\alpha_x}\right) y^{\alpha_y} \, dxdy. \tag{57}$$

Formulas (55)–(57) imply that the DoF for spaces Q_h and X_h do not depend on the rescaling operator $E_1 \to E$.

Now let us consider the following integrals:

$$\int_E p(x,y) q(x,y) \, dxdy = h^2 \int_{E_1} p_1(x,y) q_1(x,y) \, dxdy$$

and

$$\int_E \mathbf{v}(x,y)\cdot\mathbf{u}(x,y)\;dxdy = h^2\int_{E_1}\mathbf{v}_1(x,y)\cdot\mathbf{u}_1(x,y)\;dxdy.$$

Thus, we have $\mathbb{M}_{Q_E} = h^2\,\mathbb{M}_{Q_{E_1}}$ and $\mathbb{M}_{X_E} = h^2\,\mathbb{M}_{X_{E_1}}$. Since

$$\frac{1}{h^2}\int_E \mathrm{div}(\mathbf{v}(x,y))\left(\frac{x}{h}\right)^{\alpha_x}\left(\frac{y}{h}\right)^{\alpha_y}\;dxdy = \frac{1}{h^3}\int_{E_1}\mathrm{div}(\mathbf{v}(x,y))\,x^{\alpha_x}y^{\alpha_y}\;dxdy,$$

we have $\mathbb{M}_{Q_E}\,\mathbb{DIV}_E = \frac{1}{h}\,\mathbb{M}_{Q_{E_1}}\,\mathbb{DIV}_{E_1}$. This operator appears in the discrete formulation of both elliptic and parabolic problems (3) and (4).

References

[1] L. Beirão da Veiga, F. Brezzi, A. Cangiani, G. Manzini, L. D. Marini, and A. Russo. Basic principles of virtual element methods. *Math. Models Methods Appl. Sci.*, 23(1):199–214, 2013.

[2] S. Boyd and L. Vandenberghe. *Convex Optimization*. Cambridge University Press, 2004.

[3] F. Brezzi, R. S. Falk, and L. D. Marini. Basic principles of mixed virtual element methods. *ESAIM Math. Model. Numer. Anal.*, 48(4):1227–1240, 2014.

[4] B. Cockburn, J. Gopalakrishnan, and R. Lazarov. Unified hybridization of discontinuous Galerkin, mixed, and continuous Galerkin methods for second order elliptic problems. *SIAM J. Numer. Anal.*, 47(2):1319–1365, 2009.

[5] D. A. Di Pietro and A. Ern. *Mathematical aspects of discontinuous Galerkin methods*, volume 69 of *Mathématiques & Applications (Berlin) [Mathematics & Applications]*. Springer, Heidelberg, 2012.

[6] D. A. Di Pietro and A. Ern. Hybrid high-order methods for variable-diffusion problems on general meshes. *C. R. Math. Acad. Sci. Paris*, 353(1):31–34, 2015.

[7] D. A. Di Pietro, A. Ern, and S. Lemaire. An arbitrary-order and compact-stencil discretization of diffusion on general meshes based on local reconstruction operators. *Comput. Methods Appl. Math.*, 14(4):461–472, 2014.

[8] J. Droniou. Finite volume schemes for diffusion equations: introduction to and review of modern methods. *Math. Models Methods Appl. Sci.*, 24(8):1575–1619, 2014.

[9] J. Droniou and R. Eymard. A mixed finite volume scheme for anisotropic diffusion problems on any grid. *Numerische Mathematik*, 1(105):35–71, 2006.

[10] J. Droniou, R. Eymard, T. Gallouet, and R. Herbin. Gradient schemes: a generic framework for the discretisation of linear, nonlinear and nonlocal elliptic and parabolic equations. *Math. Models Methods Appl. Sci.*, 23(13):2395–2432, 2013.

[11] R. Eymard, T. Gallouët, and R. Herbin. Discretization of heterogeneous and anisotropic diffusion problems on general nonconforming meshes SUSHI: a scheme using stabilization and hybrid interfaces. *IMA J. Numer. Anal.*, 30(4):1009–1043, 2010.

[12] P. Gent and J. McWilliams. isopycnal mixing in ocean circulation models. *J. Phys. Oceanogr.*, 20:150–155, 1990.

[13] S. M. Griffies. The gent-mcwilliams skew flux. *J. Phys. Oceanogr.*, 28:831–841, 1998.

[14] V. Gyrya, K. Lipnikov, and G. Manzini. The arbitrary order mixed mimetic finite difference method for the diffusion equation. *ESAIM: Math. Mod. Numer. Anal.*, 2016.

[15] F. Hermeline. A finite volume method for the approximation of diffusion operators on distorted meshes. *J. Comput. Phys.*, 160:481–499, 2000.

[16] F. Hermeline. Approximation of diffusion operators with discontinuous tensor coefficients on distorted meshes. *Comput. Meth. Appl. Mech. Engrg.*, 192(16-18):1939–1959, 2003.

[17] G. Lin, J. Liu, and F. Sadre-Marandi. A comparative study on the weak Galerkin, discontinuous Galerkin, and mixed finite element methods. *J. Comput. Appl. Math.*, 273:346–362, 2015.

[18] K. Lipnikov, G. Manzini, and M. Shashkov. Mimetic finite difference method. *J. Comput. Phys.*, 257(part B):1163–1227, 2014.

[19] K. Lipnikov, M. Shashkov, and I. Yotov. Local flux mimetic finite difference methods. *Numer. Math.*, 112:115–152, 2009.

[20] G. Manzini, A. Russo, and N. Sukumar. New perspectives on polygonal and polyhedral finite element methods. *Math. Models Methods Appl. Sci.*, 24(8):1665–1699, 2014.

[21] M. Medvedev and V. Medvedev. Asymmetric diffusion of cosmic rays. *arXiv*, (1504.03914):1–6, 2015.

[22] V. V. Vikhrev and O. Z. Zabaidullin. Magnetic field spreading along plasma interface due to the hall effect. *Plasma Phys. Rep.*, 20:867–871, 1994.

[23] E. L. Wachspress. *A rational finite element basis*. Academic Press, Inc. [A subsidiary of Harcourt Brace Jovanovich, Publishers], New York-London, 1975. Mathematics in Science and Engineering, Vol. 114.

[24] J. Wang and X. Ye. A weak Galerkin mixed finite element method for second order elliptic problems. *Math. Comp.*, 83(289):2101–2126, 2014.

[25] A. Wilmot-Smith, E. Priest, and G. Hornig. Magnetic diffusion and the motion of field lines. *Geophysical and Astrophysical Fluid Dynamics*, 99(2):177–197, April 2005.